Proceedings of the IASS 2024 Symposium
Redefining the Art of Structural Design
August 26-30, 2024, Zurich Switzerland
Philippe Block, Giulia Boller, Catherine DeWolf,
Jacqueline Pauli, Walter Kaufmann (eds.)

Designing an ideal deformation behavior of a bending-active gridshell based on rotating quadrilaterals

Yusuke SAKAI*

* Kyoto Research, Sony Computer Science Laboratories, Inc.
13-1 Hontoro-cho, Shimogyo-ku, Kyoto 600-8086, Japan
Yusuke.C.Sakai@sony.com

Abstract

A bending-active gridshell is a curved surface elastically deformed from an initial flat grid composed of bending flexible members. The constructability of a gridshell is linked to both its grid pattern and slender beam profiles. A grid pattern composed of piecewise linear curves is difficult to be fabricated as conventional scissors' bending-active structures due to many additional parts. We introduce a bending-active gridshell exhibiting anisotropic bending deformation modes in the out-of-plane direction. This deformation behavior, referred to as mode separation, improves the constructability of a gridshell. The grid pattern is specifically designed based on a tessellation of rotating quadrilaterals. An initial flat grid is fabricated as compliant mechanism. To measure the out-of-plane deformability of the present gridshell, we compare the eigenvalues associated with elastic deformation modes. Several examples demonstrate mode separation between the out-of-plane deformation modes. By carrying out large-deformation analysis, the deformed surface with the ideal mode is investigated. Moreover, by combining rotating quadrilaterals and diagonal lines, the generated curved surfaces exhibit more complex shapes than those with uniform rotating quadrilaterals. Gridshells fabricated by 3D printer are shown for validating the results of numerical simulation. Our gridshell may provide a new insight into the design of grid pattern for generating variable shapes of bending-active gridshells with ideal deformation behaviors.

Keywords: bending-active gridshell, form-finding, grid pattern design, compliant mechanism, rotating quadrilateral, mode separation, eigenvalue analysis, large-deformation analysis

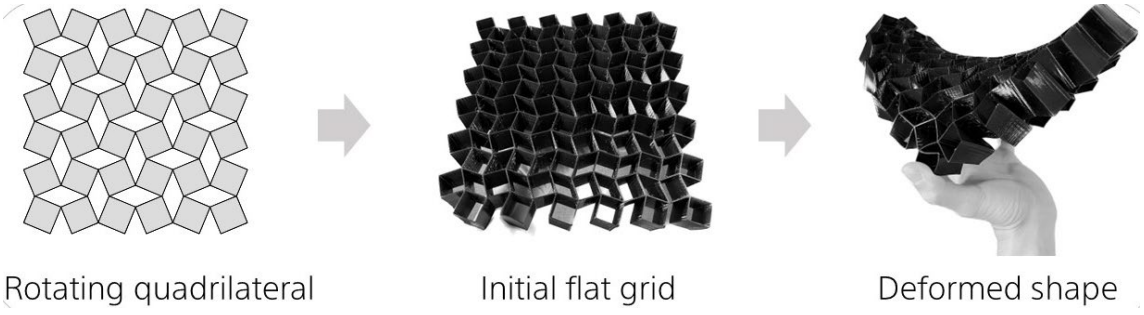

Figure 1: Design scheme of our bending-active gridshell based on rotating quadrilaterals.

1. Introduction

A bending-active gridshell is a curved surface deformed elastically from an initial flat grid composed of bending flexible beams. There has been a growing interest in rationalizing the constructability and deformability of a gridshell by focusing on its grid pattern and profile of beams [1-5]. Deformable structures combined with bending flexible beams and scissor's transformation improve the

constructability. The profile of a beam restricts its deformation degrees-of-freedom (DOF): twisting and bending deformations for in-plane and out-of-plane directions. Schikore *et al*. [1] investigates the relationships between the profile of beams and three classes of bending-active gridshells: double ruled, geodesic, and asymptotic. Nishimoto and Tachi [2] propose a shape design method of geodesic gridshell with a rhombic grid pattern. Schling *et al*. [3] and Mesnil *et al*. [4] show hybrid gridshells combined with asymptotic and geodesic ones. Their proposed gridshells are deformed easily into desirable curved surfaces.

Compliant mechanism is an alternative manufacturing technique to scissors' mechanism. By utilizing elastic deformations of a structure, compliant mechanism performs like a conventional mechanism composed of multiple rigid parts connected by hinges [6]. Using compliant mechanism for fabricating an initial flat grid, we can avoid the difficulties of a hinge: (i) losing the precise motion due to friction, (ii) increasing the total weight of a gridshell by additional parts, and (iii) assembling many beams and hinges manually. Liu *et al*. [5] propose deployable strip structures composed of thin beams fabricated as compliant mechanism. Because of the specific grid pattern composed of beams with a uniform length, their gridshells can be transformed from a fully compact state to a deployed state.

A geometrical configuration of rotating quadrilaterals is illustrated in the left figure of Fig. 1. A tessellation of rotating quadrilaterals can be transformed as a mechanism with 1 DOF [7]. Additionally, the in-plane mechanical properties of flat grids designed as the edges of rotating quadrilaterals has also been investigated [8, 9]. To the best of our knowledge, the out-of-plane deformation behavior of this class of flat grids has been still unveiled. By utilizing a geometrical configuration of rotating quadrilaterals as a grid pattern, it would be a new class of bending-active gridshells with piecewise linear curves, as shown in the center and right figures of Fig. 1.

In this paper, we propose a bending-active gridshell with a grid pattern based on a tessellation of rotating quadrilaterals. Figure 1 illustrates a design scheme of our gridshell. The geometrical configuration of an initial flat grid is designed as the edges of rotating quadrilaterals. This flat grid is fabricated monolithically like a compliant mechanism. By performing eigenvalue analysis, we investigate whether our gridshells exhibit mode separation [10], which is an ideal deformation behavior for the construction phase. Additionally, the deformed surface of a gridshell is generated by performing large-deformation analysis. Several models can deform into a curved surface close to those of the lowest out-of-plane deformation mode. To generate a more complex curved surface, we introduce a hybrid grid pattern combined with rotating quadrilateral units and their diagonal units. Finally, the deformed surfaces of numerical and physical models are compared.

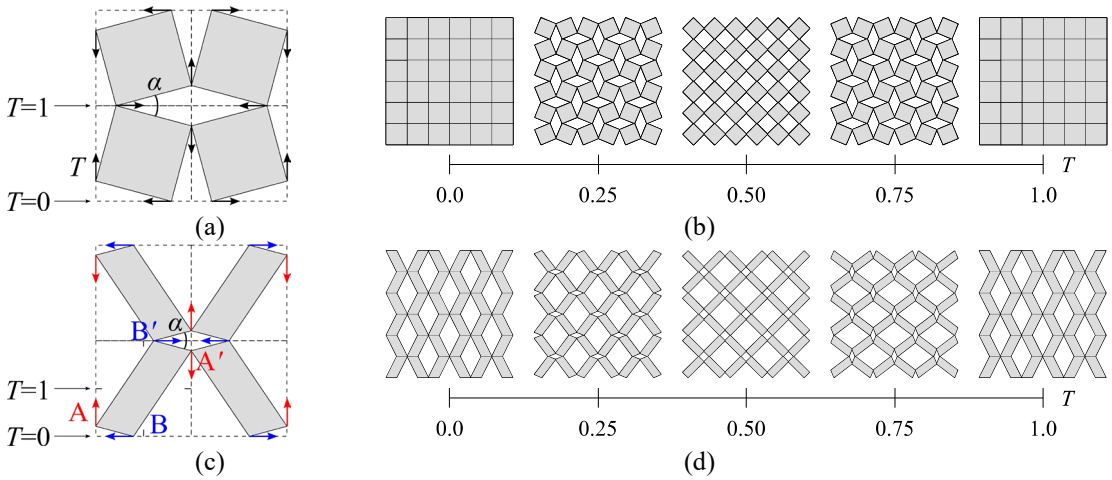

Figure 2: Geometrical configuration of rotating quadrilaterals; (a) RSUs with parameter T ($0 \leq T \leq 1$) and angle α, (b) variations of 6×6 array of RSUs, (c) RPUs with parameter T ($0 \leq T \leq 1$) and angle α, (d) variations of 6×6 array of RPUs.

2. Grid pattern based on rotating quadrilaterals

As illustrated in Fig 2, we employ a rotating square unit (RSU) [11] and rotating parallelogram unit (RPU) [12, 13] as the grid pattern. A grid pattern composed of RSUs and RPUs is tessellated by uniform quadrilaterals with reflection symmetry with respect to the dotted grid illustrated in Figs. 2(a) and (c). The geometrical configuration of a grid pattern is tuned by moving four vertices of a RSU and RPU following the arrows along the dotted grid.

2.1. Rotating square unit

As shown in Fig. 2 (a), design parameter T ($0 \le T \le 1$) determines the position of a vertex on the dotted grid. In the range of $0 < T < 1$, the grid pattern is tessellated with squares and rhombuses. When $T \in \{0, 0.5, 1\}$, the grid pattern is tessellated with uniform squares, as displayed in Fig. 2(b). The topology of a grid pattern with $T = 0$ or 1 is different from those with $T > 0$. The angle α (deg), as illustrated in Fig. 2(a), is calculated as

$$\alpha = \begin{cases} 2\arctan\left(\dfrac{T}{1-T}\right) \times \dfrac{180}{\pi} & \text{when } 0 \le T < 1 \\ 0 & \text{when } T = 1 \end{cases} \tag{1}$$

2.2. Rotating parallelogram unit

As illustrated in Fig. 2(c), the position of vertices A and A' is determined as $0.5T$, ($0 \le T \le 1$), whereas that of B and B' as $0.5(1+T)$. The topology of a grid pattern with $T > 0$ is different from that with $T = 0$, as depicted in Fig. 2(d). The angle α in the grid pattern with RPUs is also computed by Eq. (1).

3. Elastic deformation modes

An initial flat grid of our gridshell is designed as the edges extracted from an array of RSUs and RPUs. Assuming a compliant mechanism, connections between beams are monolithic without additional hinges. The cross-section of a thin beam has a rectangle with width t_b and height t_h. Following Ref. [14], eigenvalue analysis is performed for investigating the stiffness for out-of-plane deformation modes of an initial flat grid.

3.1. Eigenvalue analysis

Here, we consider an eigenvalue problem with free boundary condition. We focus on the 7th eigenmode and higher, which are called elastic modes. The eigenvalue of an elastic mode is non-zero and the deformed shape is in a stressed state. By contrast, rigid body modes, from the 1st to 6th eigenmodes, are out of scope of this study, because their eigenvalues are zero and the deformed shape is in an unstressed state.

The eigenvalue problem for an initial flat grid is written as

$$\mathrm{K}\,\mathbf{v}_i = \lambda_i \mathrm{M}\,\mathbf{v}_i \tag{2}$$

where K and M are denoted as stiffness and mass matrices, respectively. λ_i and $\mathbf{v}_i$ represent the ith eigenvalue and eigenvector, respectively. Because the components of matrix M are constant, λ_i is proportional to the components of matrix K. This means that an initial flat grid can be easily deformed into the curved surface of an elastic mode with a smaller λ_i than that with a larger λ_i.

In following examples, Abaqus Ver. 2022 [15] is used for carrying out eigenvalue analysis. The eigenvalue problem is solved by Lanczos method. We use glass fiber reinforced polymer as material with Young's modulus 25 GPa and Poisson's ratio 0.221. To reduce the deformation DOFs of an initial flat grid, the profile of a beam is set as $t_\mathrm{h} = 0.30$ (m) and $t_\mathrm{b} = 0.01$ (m), which restricts the out-of-plane bending deformation of the beam.

3.2. Out-of-plane deformation modes

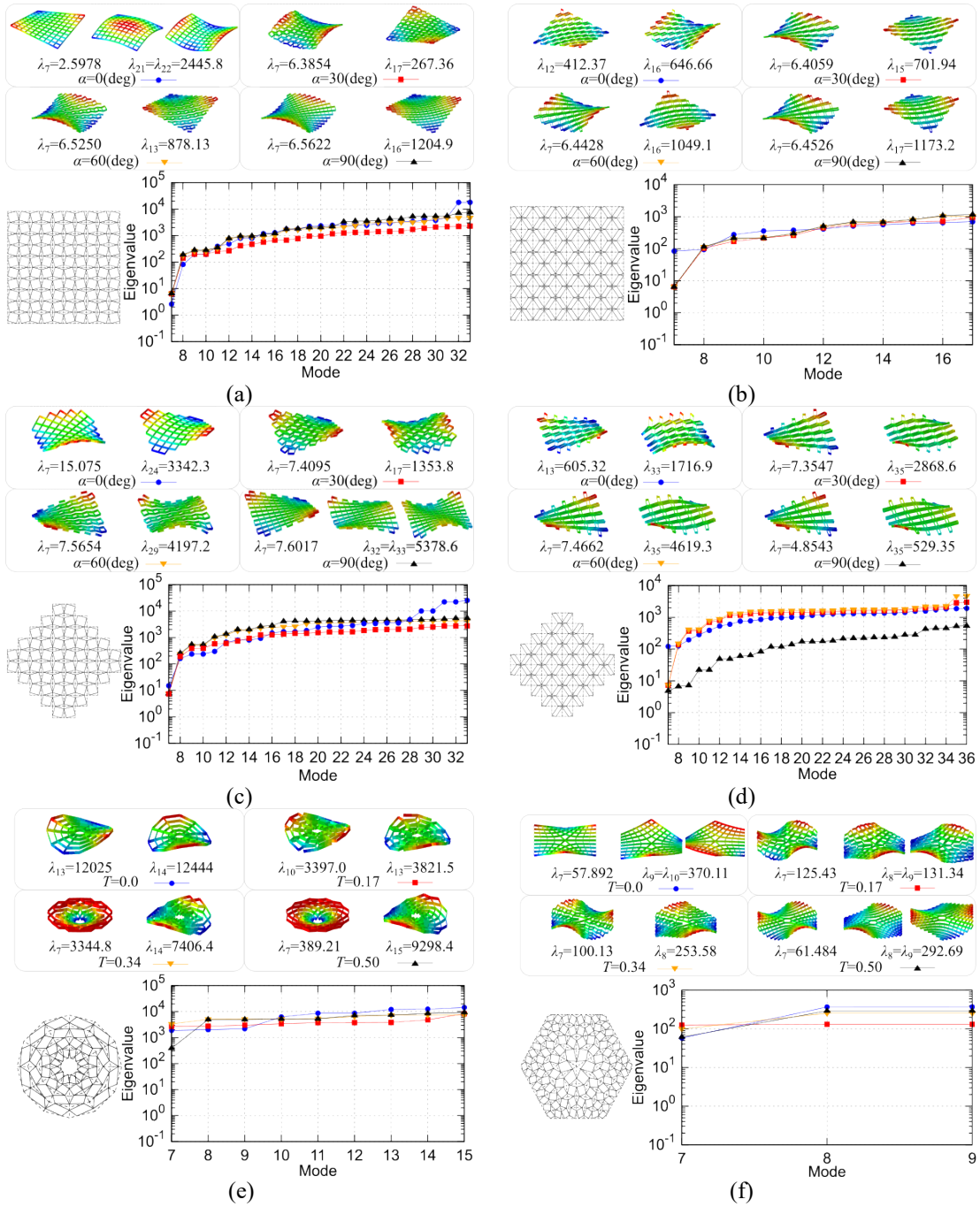

Figure 3: Comparison of eigenvalues and their corresponding deformed shapes for out-of-plane deformation modes of an initial flat grid; (a)10 × 10 array of RSUs in a rectangular boundary, (b) 10 × 10 array of RPUs in a rectangular boundary, (c) 60 RSUs in a rhombic boundary, (d) 60 RPUs in a rhombic boundary, (e) 12 × 4 array of RSUs embedded in an annulus boundary, (f) 96 RSUs embedded in a hexagonal boundary.

Figure 3 compares the deformed shapes and eigenvalues for out-of-plane deformation modes of an initial flat grid. The models shown in Figs. 3(a)–(d) are designed with the specified angle $\alpha = \{0°, 30°, 60°, 90°\}$. In contrast, the models illustrated in Figs. 3(e) and (f) are designed by specifying parameter $T = \{0.0, 0.17, 0.34, 0.50\}$. In the upper figures, the lowest and second lowest out-of-plane deformation modes are illustrated. The contour of a curved surface represents a distribution of z-directional displacement. In the lower figures, an example of the grid pattern and eigenvalues of elastic modes including both out-of-plane and in-plane deformation modes.

Figures 3(a) and (b) illustrate the models with 10×10 array of RSUs and RPUs, respectively, in a rectangular boundary with 10×10 (m). The results shown in Fig. 3(a) indicate that the lowest out-of-plane deformation modes are the 7th eigenmode for all parameters. The deformed shape of the 7th mode of the model specified with $\alpha = 0°$ is a twisted surface. In contrast, those with $\alpha = 30°$, $60°$, and $90°$ are deformed into saddle surfaces. The difference between them is caused by different topologies of their grid patterns, as explained in Sec. 2.1. Also, the results of RPUs are almost the same as those of RSUs.

As shown in Figs. 3(c) and (d), the models with 60 RSUs and RPUs, respectively, have a rhombic boundary with 10×10 (m). For both grid types, the deformed shapes of the lowest out-of-plane modes of the models with $\alpha = 0°$ are saddle surfaces, while the others are twisted surfaces.

Figure 3(e) compares the models with 12×4 array of RSUs embedded into the annulus with inner diameter 1.0m and outer diameter 6.0m. The dotted grid is aligned in the circumferential and radial directions. The deformed shapes of the lowest out-of-plane mode are saddle and cone-like surfaces. A saddle surface is deformed from an initial flat grid with $T = 0.0$ or 0.17, whereas a cone-like surface is obtained from one with $T = 0.34$ or 0.50.

As shown in Fig. 3(f), an initial flat grid with 96 RSUs is embedded into the hexagonal boundary with each side 5.0m. The dotted grid is designed by using Catmull-Clark subdivision. The deformed shapes of the lowest out-of-plane mode for the models with $T = 0.17$, 0.34, and 0.50 are saddle, whereas the deformed shape for the model with $T = 0.0$ is a twisted surface.

Table 1: Eigenvalue ratio between the lowest and second lowest out-of-plane deformation modes.

Figure	Boundary shape	Unit type	$\alpha = 0°$	$\alpha = 30°$	$\alpha = 60°$	$\alpha = 90°$
3(a)	Rectangular	RSU	941.49	41.871	134.58	183.61
3(b)	Rectangular	RPU	1.5682	109.58	162.83	181.82
3(c)	Rhombic	RSU	221.71	182.71	554.79	707.55
3(d)	Rhombic	RPU	2.8364	390.04	618.69	109.05
			$T = 0.0$	$T = 0.17$	$T = 0.34$	$T = 0.50$
3(e)	Annulus	RSU	1.0348	1.1250	2.2143	23.890
3(f)	Hexagon	RSU	6.3931	1.0471	2.5325	4.7604

For measuring the constructability of our gridshell, we calculate an eigenvalue ratio between the lowest and second lowest out-of-plane modes for an initial flat grid. Table 1 shows eigenvalue ratios for the models as investigated in Fig. 3. For instance, these eigenvalues of the model with $\alpha = 0°$ as illustrated in Fig. 3(a) are $\lambda_7 = 2.5978$ and $\lambda_{21} = \lambda_{22} = 2445.8$, respectively. The eigenvalue ratio is thus obtained as $\lambda_{21} / \lambda_7 = 941.49$. This value indicates that the stiffness required to generate a curved surface of the second lowest out-of-plane mode is 941.49 times higher than that of the lowest one. The larger ratio achieves mode separation of an initial flat grid for out-of-plane deformations.

For models corresponding to Figs. 3(a)–(d), an initial flat grid with RSUs in the rhombic boundary exhibits a larger eigenvalue ratio than one in the rectangular boundary. Also, the ratios of the initial flat grids with RPUs in the rhombic boundary are larger than those in the rectangular boundary, except the model with $\alpha = 90°$. Regarding the results of models with $\alpha = 0°$, the initial flat grids with RSUs demonstrate mode separation significantly. By contrast, those with RPUs do not exhibit mode separation clearly. These models are not easily deformed into out-of-plane deformation modes because the lowest out-of-plane modes are the 12th and 13th eigenmodes, whereas the 7th–11th eigenmodes are corresponding to in-plane deformation modes.

In contrast, an initial flat grid embedded into an annulus and hexagonal boundary exhibits a small eigenvalue ratio, because these embedded grids have higher symmetric geometries than those in a rectangular and rhombic boundary. The ratios for the models with $T = 0.0$ and 0.17 of Fig. 3(e) and that with $T = 0.17$ of Fig. 3(f) are close to 1. This relatively small value indicates that these initial flat grids can hardly achieve mode separation for out-of-plane deformations.

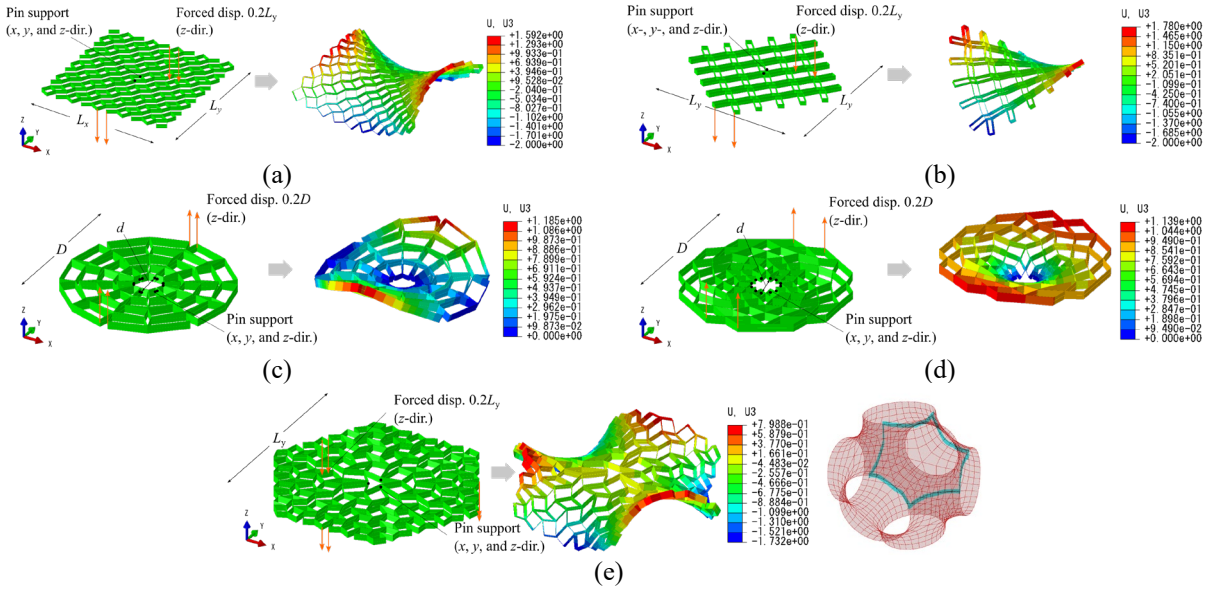

Figure 4: Initial flat grid and deformed surface under forced displacements in out-of-plane direction; (a) a saddle shape composed of 10×10 array of RSUs with $\alpha = 60°$ in the rectangular boundary, (b) a twisted shape composed of 60 RPUs with $\alpha = 60°$ in the rhombic boundary, (c) a saddle shape composed of 12×4 array of RSUs with $T = 0.10$ embedded in the annulus boundary, (d) a cone-like shape composed of 12×4 array of RSUs with $T = 0.40$ embedded in the annulus boundary, (e) a saddle shape composed of 96 RSUs with $T = 0.25$ embedded in the regular hexagon boundary, which is close to 1/8 regions of the Schwartz P surface surrounded by blue curves.

4. Relationship between a grid pattern and deformed surface

To validate the deformed shape of the lowest out-of-plane mode of the proposed initial flat grids, we investigate a relationship between a grid pattern and deformed surface. For large-deformation analysis considering geometrical nonlinearity, we carry out a quasistatic incremental path-following analysis. The loading parameter from 0.0 to 1.0 is linearly increased with the maximum increment 0.01.

4.1. Grid pattern composed of RSUs and RPUs

As shown in Fig. 4, let us consider five initial flat grids with pin-supports fixed in x, y, and z-directions at the center of a grid, represented as black circles. Forced displacements 20% of the span in y-direction, represented as orange arrows along to z-direction, are given at the boundaries.

Figures 4(a)–(e) show five initial flat grids and their deformed surfaces composed of (i) RSUs with $\alpha = 60°$ in a rectangular boundary with $L_x \times L_y = 10 \times 10$ (m), (ii) RPUs with $\alpha = 60°$ in a rhombic boundary with $L_x \times L_y = 10 \times 10$ (m), (iii) 12×4 array of RSUs with $T = 0.10$ embedded into the annulus boundary with $D = 6$ (m) and $d = 1$ (m), (iv) 12×4 array of RSUs with $T = 0.40$ embedded into the same annulus boundary as (iii), and (v) 96 RSUs with $T = 0.25$ embedded into the hexagonal boundary with 5m on each side and $L_y = 5\sqrt{3}$ (m). The contour on the deformed surface represents a distribution of z-directional displacements.

Deformed shapes of the initial flat grids in Fig. 4 are consistent with surface classes of the lowest out-of-plane deformation modes illustrated in Fig. 3. As shown in Figs. 4(a) and (b), we obtain a saddle and twisted surface, respectively. For both cases, the distance between the highest and lowest positions of the deformed surface is larger than 3.5m, i.e., 35% of the sizes of an initial flat grid in x- and y-directions. Although we assign similar boundary conditions and forced displacements, the models of Figs. 4(c) and (d) are deformed into a saddle and cone-like shape, respectively. From the result of Fig. 4(e), an initial flat grid composed of RSUs embedded into the hexagonal boundary is deformed into a saddle shape close to 1/8 parts of the Schwartz P surface.

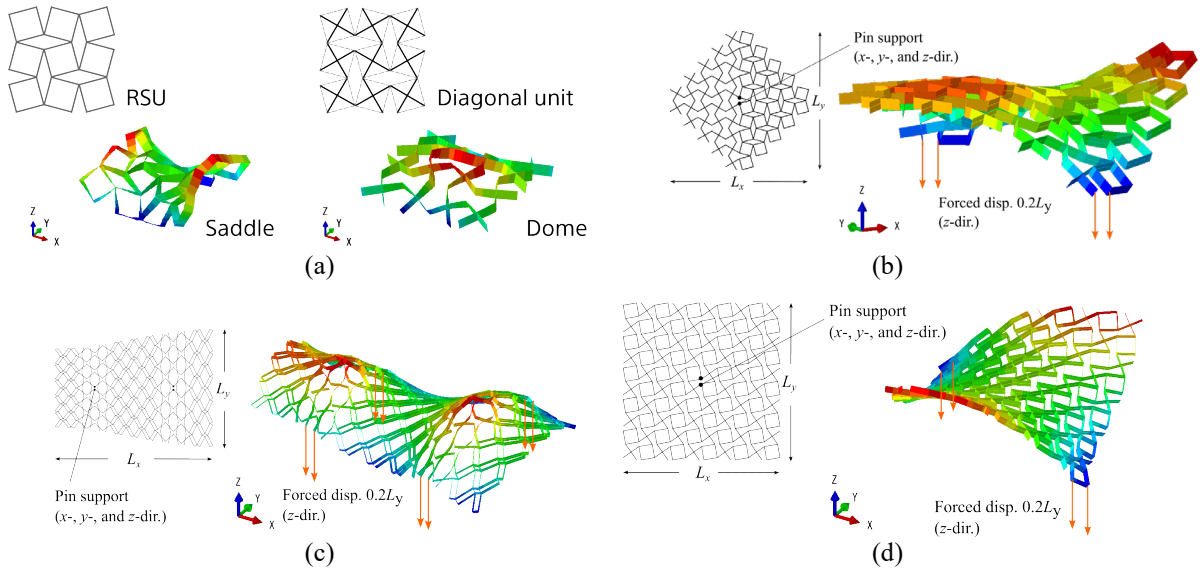

Figure 5: Hybrid grid pattern and deformed surfaces; (a) comparing deformed surfaces of RSUs and their diagonal units, (b) a curved surface composed of RSUs and their diagonal units in a rhombic boundary, (c) a curved surface composed of RPUs and their diagonal units in a tapered rectangular boundary, (d) a curved surface with a grid pattern where RSUs and their diagonal units are assigned alternately.

4.2. Hybrid grid pattern

In Secs. 3 and 4.1, rotating quadrilaterals are used for designing an initial flat grid for investigating the mechanical properties of our gridshells. In this section, we introduce a hybrid grid pattern combined with rotating quadrilateral units and their diagonal units. Figure 5(a) compares initial flat grids and deformed surfaces composed of RSUs and their diagonal units. A saddle and dome are obtained by deforming RSUs and their diagonal units, respectively, in the out-of-plane direction. By using both units for designing an initial flat grid, we therefore generate a more complex curved surface.

Figures 5(b)–(d) show hybrid grid patterns and their deformed shapes with the contour representing the distribution of z-directional displacements. To generate a curved surface, we assign forced displacements $0.2L_y$ and pin-supports fixed in x-, y-, and z-directions, represented as orange arrows and black nodes, respectively. As shown in Fig. 5(b), 30 RSUs and 30 their diagonal units are assigned to the initial flat grid in a rhombic boundary with $L_x \times L_y = 20 \times 10$ (m). The deformed surface exhibits saddle and dome on RSUs and their diagonal units, respectively. Figure 5(c) shows the gridshell composed of RPUs and their diagonal units in a tapered rectangular boundary with $L_x \times L_y = 20 \times 15$ (m). Saddle and dome are distributed alternately on their corresponding regions. Furthermore, we propose a hybrid grid pattern where RSUs and their diagonal units are assigned alternately in a rectangular boundary with $L_x \times L_y = 10 \times 10$ (m), as shown in Fig. 5(d). The deformed surface seems to be a combination of a saddle and twisted shape.

4.3. Comparison of a curved surface obtained by large-deformation analysis and 3D printed model

As displayed in Fig. 6, we compare the deformed shapes of numerical and physical models. These models are composed of (i) RSUs with $\alpha = 30°$ in a rectangular boundary with 15×15 (cm) and (ii) RSUs and their diagonal units with $\alpha = 30°$ in rectangular boundary with 15×15 (cm). Thermoplastic polyurethane (TPU95A, produced by eSUN) is used as material with Young's modulus 35MPa, Poisson's ratio 0.4, and density 1.21g/mm^3. Physical models are fabricated by using Original Prusa MK4 (produced by Prusa Research), which is based on the fused decomposition modelling. Two weights of 0.15kg are given at the center nodes on two opposite boundaries. Physical models are suspended with a string at two center nodes. For numerical models based on large-deformation analysis, we assign downward point loads 1.47N and pin-supports to these corresponding nodes.

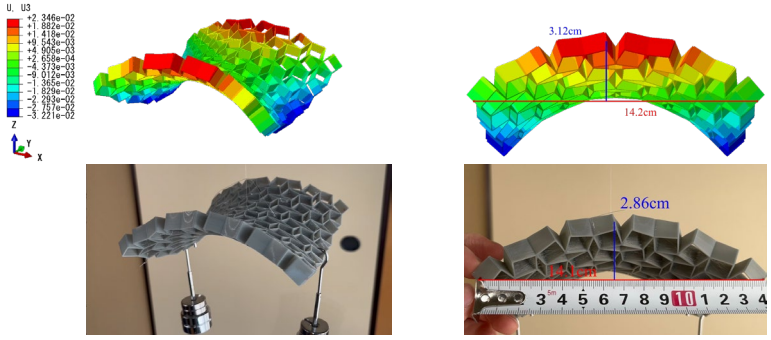

(a)

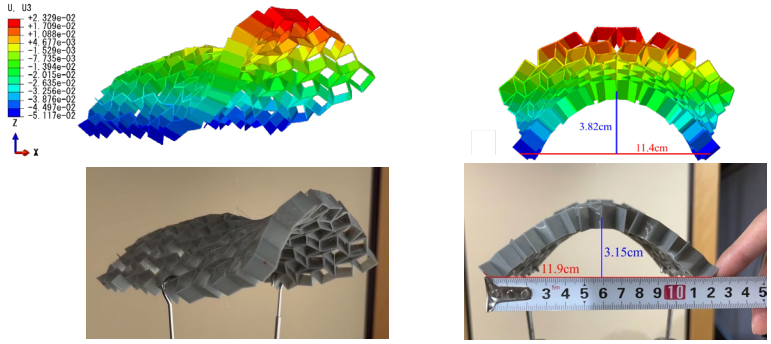

(b)

Figure 6: Comparing deformed shapes obtained by large-deformation analysis and 3D printed model; (a) 10×10 array of RSUs in a rectangular boundary, (b) 10×10 array of RSUs and their diagonal units in a rectangular boundary.

Figure 6 compares the curved surfaces obtained as numerical and physical models. The numerical model is shown in the top left figure of Figs. 6(a) and (b). The bottom left figure of Figs. 6(a) and (b) is the deformed surface of a physical model. For both cases in Figs. 6(a) and (b), the deformed surfaces of numerical and physical models are close.

As illustrated in the right figures in Figs. 6(a) and (b), we measure the spans, indicated by red lines, between nodes at two corners of deformed numerical and physical models. The rises, highlighted by blue lines, are calculated based on the difference between lengths of red and blue lines. For the physical model of Fig. 6(a), the span and rise of a deformed surface are measured as 14.1cm and 2.86cm, respectively. Those of the model obtained by large-deformation analysis are computed as 14.2cm and 3.12cm. In the bottom right figure in Fig. 6(b), the span and rise are measured as 11.9cm and 3.13cm, respectively. The corresponding distances of numerical models are 11.4cm and 3.82cm. The relative errors for Fig. 6(a) are approximately 0.71% for the span and 9.09% for the rise, whereas for Fig. 6(b), they are approximately 4.2% for the span and 22.05% for the rise. For both cases, the errors for the rise are larger than those for the span.

5. Conclusions

We proposed a bending-active gridshell with a grid pattern based on rotating quadrilaterals. An initial flat grid is composed of RSUs and RPUs. The geometrical configuration of an initial flat grid is adjusted by shape parameter. To restrict the deformation DOFs of an initial flat grid, a beam has a thin rectangular cross-section that allows in-plane bending and twisting deformations. Additionally, we utilize the eigenvalue ratio between the lowest and second lowest out-of-plane modes as an indicator for mode separation of an initial flat grid. Most of the models in a rectangular and rhombic boundary can produce significant mode separation. Moreover, we proposed a hybrid grid pattern for generating a more complex curved surface. By adjusting the arrangement of both quadrilateral and diagonal units, a curved surface has a more complex shape than that deformed from an initial flat grid composed of only RSUs and RPUs. We compared the deformed shapes of numerical and physical models. The span and rise of the numerical and physical models have slight differences. It has left room for improving the accuracy of the

measurement by employing digital tools such as 3D scanning and photogrammetry. However, the overall shapes are close for both cases. For large-scaled architectures, braces are incorporated to reinforce both in-plane and out-of-plane stiffness in the deployed state. This investigation will enhance our understanding of a gridshell with an ideal deformation behavior for its construction.

References

[1] J. Schikore, E. Schling, T. Oberbichler and A. M. Bauer, "Kinetics and design of semi-compliant grid mechanisms," *In Proceedings of Advances in Architectural geometry 2021,* pp. 108-129, 2021.

[2] S. Nishimoto and T. Tachi, "Transformable surface mechanisms by assembly of geodesic grid mechanisms," *In Proceedings of the Advances in Architectural Geometry 2023,* pp. 221-234, 2023.

[3] E. Schling, H. Wang, S. Hoyer and H. Pottmann, "Designing asymptotic geodesic hybrid gridshells," *Computer-Aided Design,* 152, 103378, 2022.

[4] R. Mesnil and O. Baverel, "Pseudo-geodesic gridshells," *Engineering Structures,* 279, 115558, 2023.

[5] D. Liu, D. Pellis, YC. Chiang, F. Rist, J. Wallner and H. Pottmann, "Deployable strip structures," *ACM Transactions on Graphics,* vol. 42(4), no. 106, pp.1-16, 2023.

[6] L. L. Howell, "Compliant Mechanisms," *Wiley,* 2001.

[7] J. N. Grima, A. Alderson and K. E. Evans, "Auxetic behaviour from rotating rigid units," *Physica Status Solidi (b),* 242(3), pp. 561-575, 2005.

[8] M. Chen, J. Huang, W. Jiang and M. Fu, "Elastic properties of lightweight rotating square structures," *Materials Today Communications,* vol. 33, 104256, 2022.

[9] L. Mizzi and A. Spaggiari, "Lightweight mechanical metamaterials designed using hierarchical truss elements," *Smart Materials and Structure,* 29(10), 105036, 2020.

[10] T. Tachi, "Introduction to structural origami," *Journal of the International Association for Shell and Spatial Structures,* vol. 60, no. 199, pp. 7-18, 2019.

[11] J. N. Grima and K. E. Evans, "Auxetic behaviour from rotating squares," *Journal of Materials Science Letters,* 19, pp. 1563-1565, 2000.

[12] D. Attard, E. Manicaro and J. N. Grima, "On the rotating rigid parallelograms and their potential for exhibiting auxetic behaviour," *Physica Status Solidi (b),* 246(9), pp. 2033-2044, 2009.

[13] Y. Zheng, I. Niloy, P. Celli, I. Tobasco and P. Plucinsky, "Continuum field theory for the deformations of planar kirigami," *Physical Review Letters,* 128, 208003, 2022.

[14] E. T. Filipov, T. Tachi and G. H. Paulino, "Origami tubes assembled into stiff, yet reconfigurable structures and metamaterials," *Proceedings of the National Academy of Sciences,* 112(40), pp. 12321-12326, 2015.

[15] Dassault Systems, "Abaqus 2022 User's Manual," 2022.

Proceedings of the IASS 2024 Symposium
Redefining the Art of Structural Design
August 26-30, 2024, Zurich Switzerland
Philippe Block, Giulia Boller, Catherine De Wolf,
Jacqueline Pauli, Walter Kaufmann (eds.)

Copyright Declaration

Before publication of your paper in the Proceedings of the IASS Annual Symposium 2024, the Editors and the IASS Secretariat must receive a signed Copyright Declaration. The completed and signed declaration may be uploaded to the EasyChair submission platform or sent as an e-mail attachment to the symposium secretariat (papers@iass2024.org). A scan into a .pdf file of the signed declaration is acceptable in lieu of the signed original. In the case of a contribution by multiple authors, either the corresponding author or an author who has the authority to represent all the other authors should provide his or her address, phone and E-mail and sign the declaration.

Paper Title: Designing an ideal deformation behavior of a bending-active gridshell based on rotating quadrilaterals

Author(s): Yusuke SAKAI

Affiliation(s): Kyoto Research, Sony Computer Science Laboratories, Inc.

Address: 13-1 Hontoro-cho, Shimogyo-ku, Kyoto-shi, Kyoto, Japan

Phone: (+81)75-456-1001

E-mail: Yusuke.C.Sakai@sony.com

I hereby license the International Association for Shell and Spatial Structures to publish this work and to use it for all current and future print and electronic issues of the Proceedings of the IASS Annual Symposia. I understand this licence does not restrict any of the authors' future use or reproduction of the contents of this work. I also understand that the first-page footer of the manuscript is to bear the appropriately completed notation:

> *Copyright © 2024 by Yusuke SAKAI*
> *Published by the International Association for Shell and Spatial Structures (IASS) with permission*

If the contribution contains materials bearing a copyright by others, I further affirm that (1) the authors have secured and retained formal permission to reproduce such materials, and (2) any and all such materials are properly acknowledged by reference citations and/or with credits in the captions of photos/figures/tables.

Printed name: Yusuke Sakai

Signature: Yusuke Sakai

Location: Kyoto, Japan

Date: 2024/06/28